Hierarchical Self-Assembly of Gold Nanoparticles into Patterned Plasmonic Nanostructures

Cyrille Hamon,[†] Sergey Novikov,[†] Leonardo Scarabelli,[†] Lourdes Basabe-Desmonts,[‡,§] and Luis M. Liz-Marzán[*,†,§]

[†]Bionanoplasmonics Laboratory, CIC biomaGUNE, Paseo de Miramón 182, 20009 Donostia-San Sebastian, Spain, [‡]BIOMICs Research Group, Lascaray Ikergunea Research Center, University of the Basque Country, Euskal Herriko Unibertsitatea, UPV-EHU, Vitoria, Spain, and [§]Ikerbasque, Basque Foundation for Science, 48011 Bilbao, Spain

ABSTRACT The integration of nanoparticle superstructures into daily life applications faces major challenges including the simplification of the self-assembly process, reduced cost, and scalability. It is, however, often difficult to improve on one aspect without losing on another. We present in this paper a benchtop method that allows patterning a macroscopic substrate with gold nanoparticle supercrystals in a one-step process. The method allows parallelization, and patterned substrates can be made with high-throughput. The self-assembly of a variety of building blocks into crystalline superstructures takes place upon solvent evaporation, and their precise placement over millimeter scale areas is induced by confinement of the colloidal suspension in micron-sized cavities. We mainly focus on gold nanorods and demonstrate their hierarchical organization up to the device scale. The height of the formed nanorod supercrystals can be tuned by simply varying nanorod concentration, so that the topography of the substrate and the resulting optical properties can be readily modulated. The crystalline order of the nanorods results in homogeneous and high electric field enhancements over the assemblies, which is demonstrated by surface-enhanced Raman scattering spectroscopy.

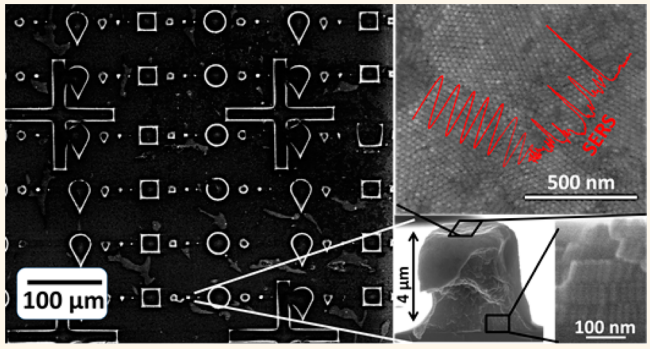

KEYWORDS: gold nanorods · hierarchical organization · smectic ordering · surface patterning · SERS · self-assembly

On the way toward practical implementation of nanostructured devices, increasing interest has been placed on the design of multifunctional platforms. The surface chemistry and composition of such smart materials can be tuned to induce properties like localized heating, sensing, or target trapping and release on the same spot.[1−8] These systems have been used for ultratrace detection of molecular targets and show promise in various technologies ranging from medicine to homeland security.[9−11] Therefore, there is large interest in combining the properties of nanostructured materials with an overall control of the topography in order to manufacture (bio)active surfaces. This emerging class of materials can interact with analytes of different sizes ranging from small proteins to living cells, thanks to the modulation of surface chemistry as well as the topography of the substrate. In this last case, the topography is an important parameter to direct the fate of living cells as it can modulate their adhesion, which is important, for example, in tissue engineering.[4,12,13] On the other hand, such implementation would require the fabrication of patterned surfaces with high-throughput, which could be used in various fields such as nonfouling surfaces,[14] antimicrobial materials,[15] or biosensor component design,[6,16,17] among others. The present work describes a methodology based on using nanoparticles as elementary building blocks to manufacture functional hierarchical materials over extended surface areas.

Surface topography can be modulated by a variety of methods such as soft lithography, which allow a fine control over the

* Address correspondence to llizmarzan@cicbiomagune.es.

Received for review August 7, 2014 and accepted September 28, 2014.

Published online September 29, 2014
10.1021/nn504407z

morphology of pattern features. Nanofabrication techniques[18−21] such as stamping[22] or micromolding in capillary[23] have been explored for the assembly of polymers,[24] polystyrene beads,[25] and inorganic particles[20] as well as to perform chemical reactions *in situ*.[23] In parallel, the preparation of crystalline assemblies of nanoparticle building blocks (supercrystals) has quickly evolved due to the resulting collective properties, which are highly beneficial over those of the individual particles.[26] In the particular case of gold nanoparticles (GNPs), supercrystals display collective plasmon resonances resulting from plasmon coupling that gives rise to intense and highly localized electromagnetic fields.[6,10,17,27] Raman scattering or fluorescence signals of target analytes can be enhanced by such fields, leading to ultratrace and even single-molecule detection.[10,28−32] With the aim of designing a multifunctional platform that combines structural tunability at the macroscale and sensing properties, we developed an approach that takes advantage of both GNP self-assembly and the surface tunability of soft lithography techniques.

Several approaches have been reported that combine soft lithography and evaporative self-assembly, which may be classified according to the dimensions of the pattern. Controlled evaporation within a pattern having dimensions on the order of magnitude of the particles has been used to form monolayers of discrete building blocks.[33−37] For example, Zhou *et al.*[33] used an elastomeric template to selectively assemble single gold particles according to their shape and size, over several micrometers, using microcontact printing to transfer the particle monolayer onto a substrate of interest. A second group of techniques comprises the use of patterns that have wider dimensions than the individual building blocks, from which supercrystals can be built.[38,39] In this respect, Thai *et al.*[38] reported the assembly of gold nanorods into small supercrystals within a silicon pattern having different wettability properties. In this case, the pattern was not reusable. Nanoparticles can also be evaporated directly on a substrate by using a template having significantly larger dimensions than the building blocks.[40−43] Large supercrystals have been built in this way, even in one-step processes. Hamon *et al.*[41] reported the controlled evaporation of a suspension of gold nanorods between micron-sized pillars on a substrate, resulting in a three-dimensional maze. However, the lack of both precision and predictable localization of the supercrystals was a clear limitation of this device fabrication strategy. Another study used field-directed assembly of spherical nanoparticles on poly(methyl methacrylate) templates to form micropillars, which required a number of processing steps as well as the destruction of the template and a complex setup.[42] All of the above examples do not address three of the major challenges toward the integration of nanoparticle superstructures into commercially viable applications, that is, simplification of the self-assembly process, reduced cost, and scalability.[44] Unfortunately, improving the scalability often involves the use of more complex setups, in turn increasing the overall cost. The design of a technique combining these three aspects would thus be highly relevant in fields ranging from optoelectronics to the fabrication of bioactive surfaces.

We present in this paper a simple method that allows patterning arbitrary substrates with gold nanoparticle supercrystals over large areas through a one-step process. To tackle problems of reproducibility occurring in previously reported methods, we used an elastomeric template made of polydimethylsiloxane (PDMS) displaying arrays of micron-sized cavities that help to regulate the evaporation of the GNP colloid directly on a substrate of interest. We thereby achieved a high control over supercrystal morphology and tuned the topography of the patterned substrate on the millimeter scale. We additionally demonstrate that the prepared supercrystals show high homogeneity and can be used for highly sensitive SERS detection. Overall, we show an unprecedented fine-tuning of the supercrystal dimensions over large areas, which can be implemented using a wide variety of plasmonic nanoparticles and in a single-step process. The robustness, simplicity, versatility, and reusability of the templates, as well as the potential parallelization of the method, constitute a significant step forward in the development of large-area substrates for plasmonic sensing. Thus, this multifunctional platform may result of great relevance for new strategies toward the design of point-of-care devices.

RESULTS AND DISCUSSION

Nanoparticles of different shapes and sizes were synthesized as building blocks for the formation of supercrystal arrays. We prepared 17 ± 2 nm diameter gold nanoparticles and two different types of GNRs with different dimensions. Smaller, single-crystal GNRs (55 ± 6 nm length; 17 ± 2 nm width) were synthesized following a seed-mediated process involving a prereduction step with salicylic acid. This high-yield synthesis developed by Murray and co-workers[45] and refined by our group[46] yielded GNRs with high monodispersity, which is crucial for high-quality self-assembly.[6,47] In all cases, the capping ligand used for the synthesis, cethyltrimethylammonium bromide (CTAB), was exchanged with (1-mercaptoundec-11-yl)hexa(ethylene glycol) (MUDOL), a commercially available amphiphilic ligand bearing a thiol moiety (Figure 1a). MUDOL has been reported to cap GNRs, and it is known to induce smectic order upon solvent evaporation.[41,48] The functionalization and characterization of the synthesized GNRs is described in the Supporting Information (Figures S1−S4). Notably, the formation of a homogeneous superlattice of standing rods was evidenced

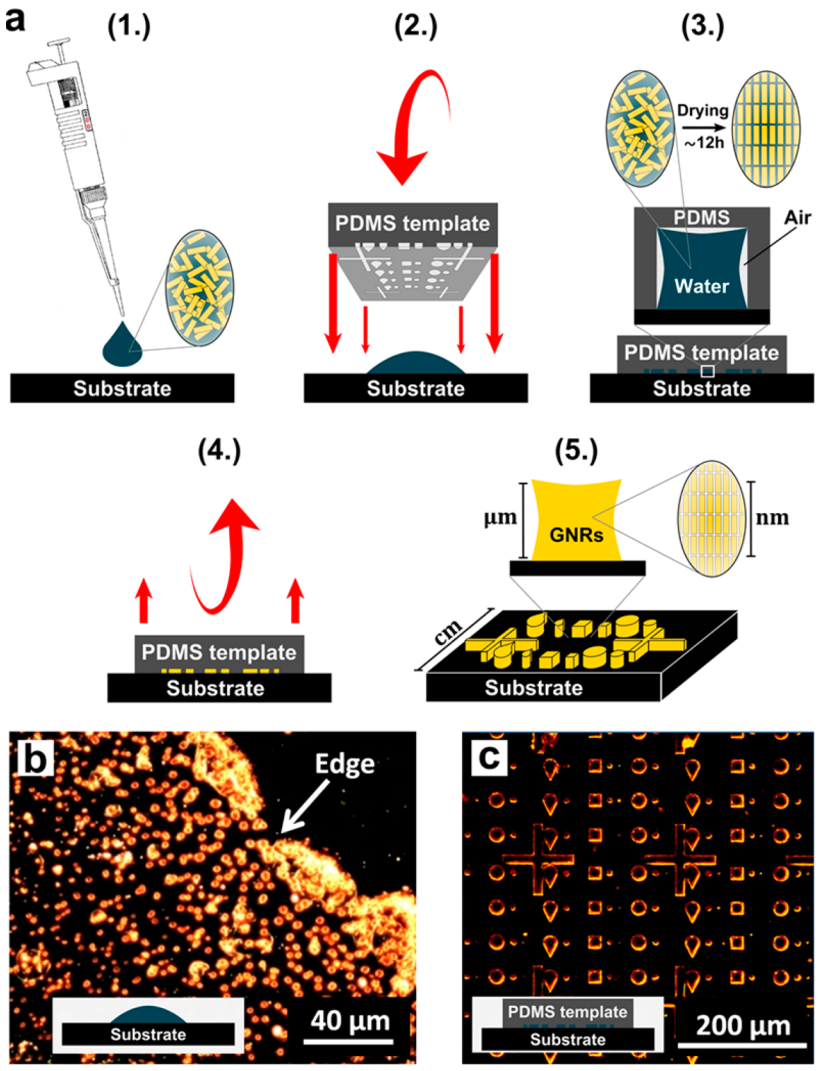

Figure 1. (a) Schematic view of the PDMS template-driven self-assembly process. (1) A 2 μL GNR suspension was drop-casted with a micropipette on a substrate. (2) Then a PDMS template displaying arrays of cavities was stamped on the substrate. (3) The wetting properties of the suspension were modulated by the template, and a meniscus formed at the triple contact line between air, solution, and substrate directed the supercrystal shape after drying. The solvent was allowed to evaporate for 12 h, allowing the crystallization of gold nanorods into smectic phases. (4) The template was then removed, and (5) arrays of gold nanorod supercrystals were obtained over the substrate. All nanoparticles were functionalized with (1-mercaptoundec-11-yl)hexa(ethylene glycol), denoted as MUDOL. Different substrates were employed such as glass slides, silicon wafers, or TEM grids. (b–c) Dark-field images of GNR supercrystals on glass obtained by drop-casting (b) or PDMS template-driven self-assembly (c). Drop-casting yielded a macroscale assembly determined by the coffee stain effect, resulting in accumulation of GNPs at the edge of the drop.

for MUDOL–GNR, whereas CTAB–GNRs were arranged into poorly ordered arrays under the same conditions. Therefore, all nanoparticles used for this work were functionalized with MUDOL using the same procedure.

When GNRs self-assemble on a flat substrate by drop-casting, supercrystals are formed upon drying with a random organization and a wide distribution of supercrystal sizes but mostly with circular shape. Additionally, due to the coffee stain effect,[49] the density of supercrystals was found to be larger at the edge of the drop (Figure 1b). Aiming at controlling the morphology (size and shape) as well as the local organization of the supercrystals, a PDMS template was used, which affected the evaporation of the solvent at certain places on flat substrates. The PDMS templates comprised an array of cavities with various shapes and sizes, but with a fixed depth of 4.8 μm. Images of a typical PDMS template are shown in the Supporting Information (Figure S5). Initially, we used a template displaying cavities with four different dimensions of 2, 6, 12, and 20 μm in diameter, in arrays of three different cavity shapes: circle, square, and drop (Figure 1c). For the formation of the assemblies, a drop of GNR suspension was confined between the mold and a flat substrate (glass, silicon, or even TEM grids), and the system was then allowed to dry overnight under ambient conditions, as schematically depicted

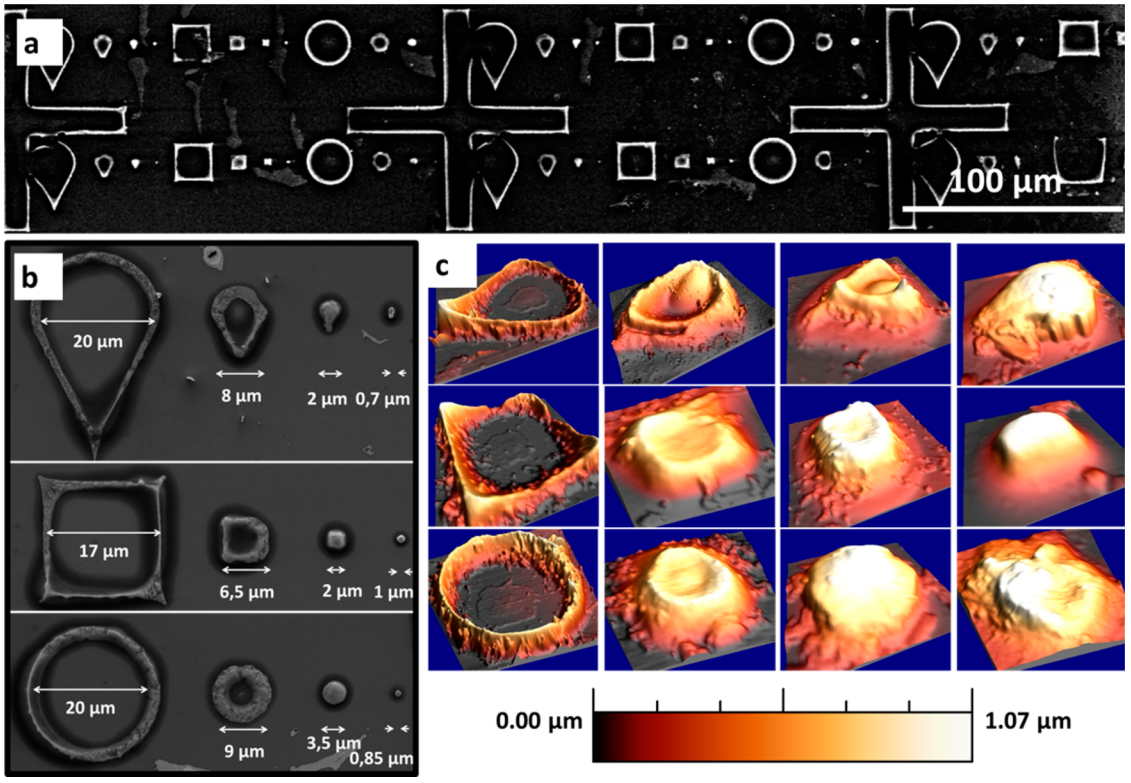

Figure 2. Nanoparticle supercrystal arrays formed by PDMS template-driven assembly. The resulting arrays comprised supercrystals of different shapes and dimensions, ranging from 700 nm to 20 μm. (a) SEM of a GNR supercrystal array showing the long-range order of micron-scale features at device scale on a glass slide. (b) SEM images at higher magnification show the nanoscale topography of the substrate. The sizes are indicated below each supercrystal. (c) Three-dimensional AFM topography plots of the supercrystals obtained from cavities with different shapes and sizes. A rounded hollow area is clearly visible on top of big supercrystals, whereas smaller ones are full of particles.

in Figure 1a. Subsequently, the PDMS template was carefully removed, and well-defined supercrystal arrays were formed with dimensions that replicated those of the mold cavities (Figure 1c). Interestingly, the relative orientation of the substrate, either being on the top or on the bottom of the assembly setup, did not seem to affect particle deposition and organization (Figure 1a). It is important to note that the particles invariably deposited on the substrate rather than on the PDMS template, presumably because of the wettability contrast between the hydrophilic substrate and the hydrophobic mold.

Low-magnification dark-field optical microscopy images of the glass substrate demonstrate the long-range order and the homogeneity of the micron-scale features within the array, meaning that the supercrystals were regularly patterned over the substrate in the millimeter scale (Figure 1c). In comparison with the drop-casting method, a remarkable improvement of the homogeneity and long-range order can be clearly observed. The assembly process resulted in an accurate reproduction of the geometry of the cavities in the PDMS mold, forming circles, squares, and drop-shaped supercrystals (Figure 2a,b). An additional observation is that the degree to which the cavities were filled, as well as the detailed morphology of the supercrystals, depended on the lateral dimensions of the cavities in the PDMS template. Whereas supercrystals formed in wider cavities of 20 and 12 μm displayed a middle hole, those assembled in smaller cavities of 6 and 2 μm wide were fully packed with nanoparticles (Figure 2b,c). It was also found that, except for the larger cavities (20 μm), the average size of the formed supercrystals was smaller than the initial cavity size. The supercrystals formed from the widest cavities, however, retained the size of the template cavity. We argue that confinement in smaller cavities increases the interaction between the aqueous dispersion and the hydrophobic template, leading to more constrained menisci and shrinkage during drying and self-assembly. In agreement with this interpretation, supercrystals usually displayed rounded profiles (Figure 2c), which may be seen as reminiscent of a meniscus formed at the triple contact line between air, the solution, and the substrate. PDMS is known to be hydrophobic with a water contact angle of $\approx$110°,[19] thus the GNR suspension was likely not to fully wet the cavities and form a meniscus during assembly. We attempted to make supercrystals that better fit the cavity shapes by adding a surfactant to change the wettability of the aqueous colloid. Polysorbate 20 (T20)[41,43] was added to the GNR colloid above

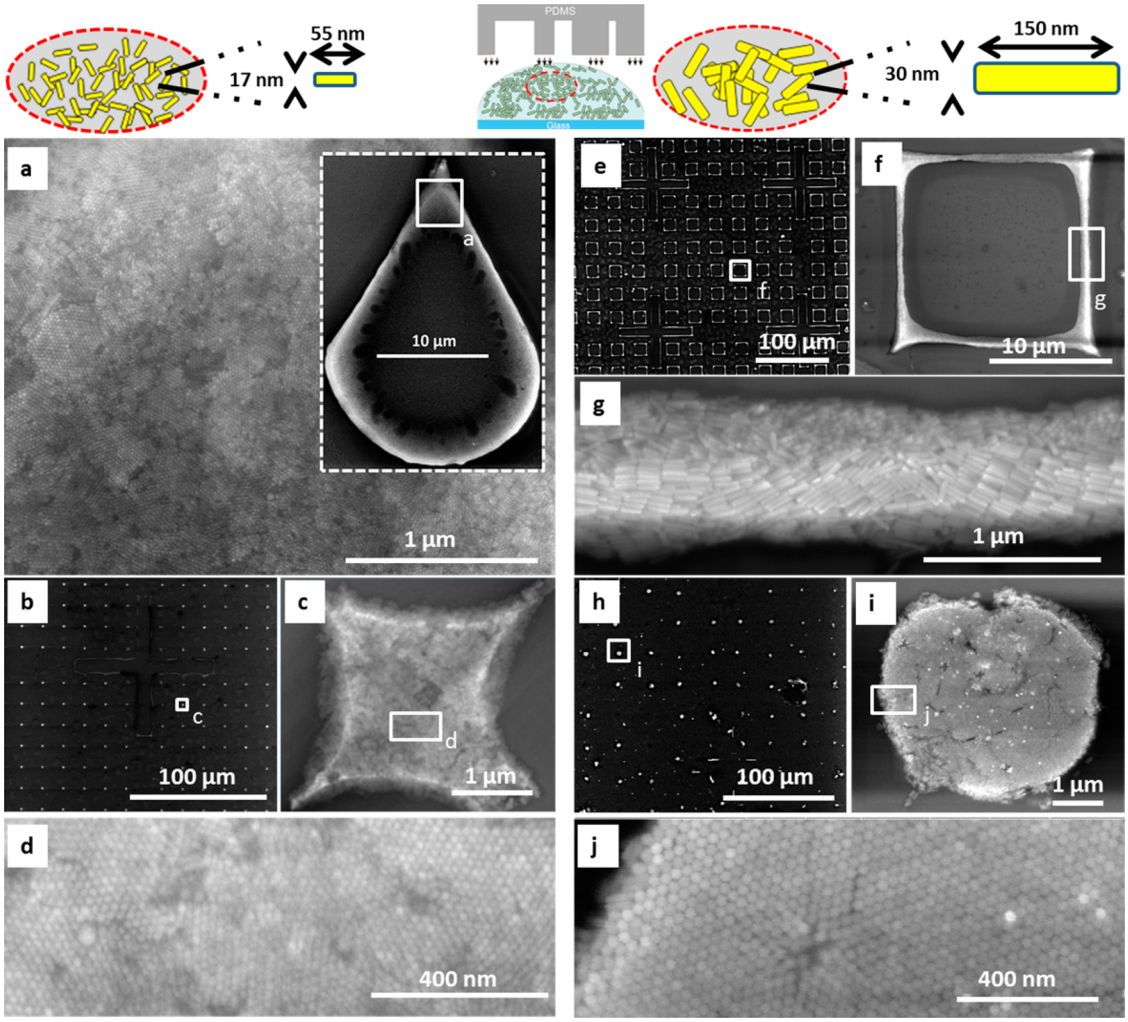

Figure 3. Multiscale SEM characterization of patterned substrates obtained by PDMS-driven self-assembly. Patterned substrates were obtained from colloidal solutions of GNRs of different dimensions: 55 × 17 nm (a–d) and 150 × 30 nm (e–j). Images were selected to represent supercrystals made from cavities with different size and shape: (a) drop-shaped cavity with 20 μm diameter; (b–d) square with 2 μm diameter; (e–g) square with 20 μm diameter; (h–j) circle with 6 μm diameter.

its critical micelle concentration, but no significant changes in the supercrystal shape were noticed. Another strategy would involve lowering the hydrophobicity of the mold, for example, by treating it with oxygen plasma prior to the assembly process, but such a detailed investigation was beyond the focus of the proof of concept study reported here.

PDMS template-driven assembly was applied to (MUDOL-capped) gold nanoparticles with different morphologies, such as size and aspect ratio, which also resulted in the formation of supercrystals. We used spheres (AR = 1) with 17 nm diameter, low aspect ratio GNRs (55 × 17 nm, AR = 3.2), and high aspect ratio GNRs (150 × 30 nm, AR = 5). In all cases, the macroscale organization was found to accurately reproduce the template geometry (Figures 3 and S6). However, the degree of local order of the building blocks varied depending on their dimensions. Spheres and low aspect ratio nanorods formed hexagonal lattices regardless of the template geometry and dimensions (Figures 3a–d and S6). On the other hand, longer nanorods showed different organization depending on the size of the template cavity. Interestingly, we observed hexagonal packing when smaller cavities were used but significantly less ordered assemblies for larger cavities (Figure 3e–j), where both standing and lying GNRs were present in the superlattices (Figure 3g,j). This effect is probably related to the action of capillary forces inside the cavities during the assembly of this type of nanorod during drying. It should be noted, however, that such longer nanorods display pentagonal cross section, which may also affect their self-assembly, as compared to single-crystal nanorods, which have more rounded cross sections (Figure S7). Another possible reason behind the different local organization of the two types of nanorods is the change in aspect ratio, 3.2 *versus* 5.[50] Overall, this last set of experiments demonstrates the versatility of the technique as it was applied to particles with different size and shape. Naturally, the organization of the

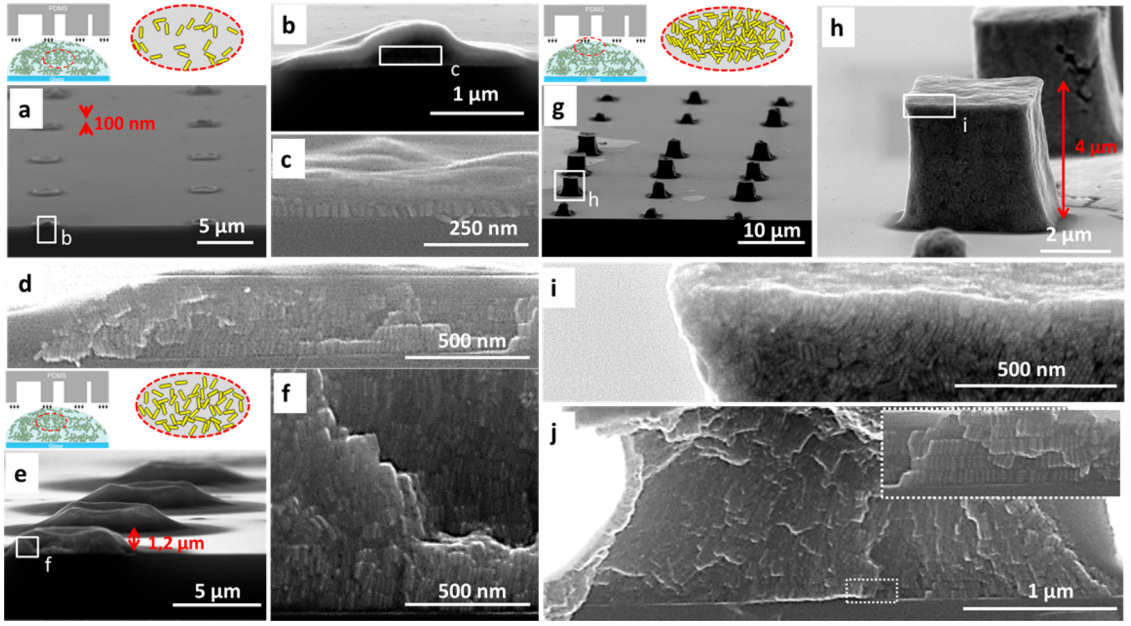

Figure 4. SEM characterization of patterned substrates obtained at different GNR concentrations of 15 mM (a−c), 24 mM (d), 75 mM (e,f), and 375 mM (g−j). GNR concentration is expressed as Au^0 molar concentration. Substrates were cleaved and imaged with a tilt angle of 35°.

nanoparticles within the supercrystals could be optimized, for example, by using more extended drying times,[6,17,51] perhaps employing evaporation chambers with controlled humidity and temperature. In the present work, we found that, by using the PDMS templates, nanoparticle crystallization could be achieved within drying times in the range of 12 h under ambient conditions.

The concentration of nanoparticles in the colloidal dispersion was found to have a strong influence on the formation of supercrystal arrays. We restrict this analysis to short GNRs (55 × 17 nm, AR = 3.2) because they form supercrystals with a homogeneous organization and also because they have been demonstrated to perform better than their spherical counterparts for sensing applications.[6] In the following, the GNR concentration is expressed in molar concentration of Au^0, extracted from the absorbance at 400 nm.[46] Supercrystal arrays were prepared on silicon wafers using GNR concentrations in water of 15, 75, and 375 mM. The assemblies were characterized by SEM at different tilt angles with respect to the substrate, while the inner structure of the supercrystals was investigated by carefully cleaving the substrate (Figure 4). The top view of the corresponding supercrystals is shown in the Supporting Information (Figure S8).

When the initial GNR concentration was as low as 15 mM and the cavities were large (20 μm in diameter), discrete supercrystals deposited as discontinuous lines along the edge of the template structure (Figure S9). On the contrary, supercrystals with larger particle density were obtained when small cavities (2 μm diameter) were used. Interestingly, the height of these supercrystals (50−100 nm) corresponds to mono- and bilayers of standing GNRs (Figure 4c). Additional characterization was carried out by forming the supercrystal arrays on a TEM grid, which allowed us to determine a spacing between nanorods of *ca.* 2 nm, in agreement with the replacement of the CTAB bilayer with MUDOL (Figure S10). Increasing the GNR concentration up to 75 mM induced the formation of uniform assemblies that follow the template geometry for all cavity sizes, which also contained a larger number of GNR monolayers (1.2 μm height; see Figure 4e). Finally, for even higher GNR colloid concentration of 375 mM, uniform assemblies were also observed, but GNR monolayer deposition was also observed outside the limit of the cavities (Figure S8). In this case, the height of the supercrystals was around 4 μm (Figure 4h). In all cases, investigation of the inner structure of the supercrystals revealed smectic order with nanorods vertically oriented with respect to the substrate (Figure 4c,d,f,j). The average number of layers was around 1−2, 20, and 70 for GNR concentrations of 15, 75, and 375 mM, respectively. Therefore, the optimal concentration was found to be around 75 mM because it leads to homogeneous deposition of nanorods for all cavity sizes. It should be noticed that such supercrystal size is difficult to obtain by other techniques unless very high GNR concentrations are used. In the present work, the supercrystals' height was modulated between 0.1 and 4 μm using moderate (between 15 and 375 mM) GNR concentration and the same mold in the self-assembly process. The smectic B organization of the nanorods within the supercrystals was demonstrated by observation of hexagonal and lamellar order when they are

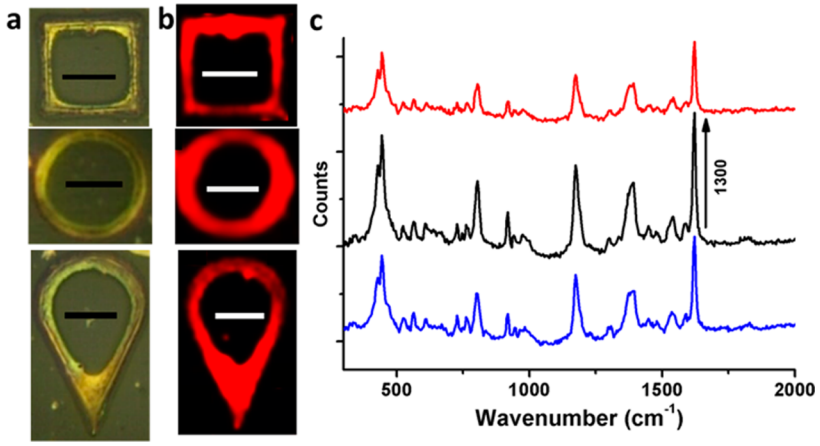

Figure 5. Optical microscopy images (a) of GNR supercrystals and corresponding SERS images (b) obtained by mapping the intensity of the crystal violet vibrational peak integrated over 1618−1632 cm^{-1}. The scale bar on all images is 10 μm. (c) Average SERS spectra of crystal violet at a concentration of 10^{-6} M in ethanol, drop-casted on the substrate and dried under ambient conditions. Spectra were acquired on supercrystals with different shapes: drops (blue), circles (black), and squares (red). The acquisition time was 500 ms, and the laser power was ≈0.15 mW at an excitation wavelength of 633 nm. Spectra were vertically shifted for the sake of clarity. The total number of counts is indicated by a black arrow corresponding to the intensity of the peak at 1626 cm^{-1}.

characterized from the top and from the edge of the supercrystals, respectively. This type of organization is particularly suited for sensing applications as the high particle density maximizes hot-spot formation at multiple gaps between nanorods.[6,27]

After optimization of the patterned self-assembly process, we examined the sensing properties of the nanoparticle supercrystals on the basis of the well-known efficiency of these systems toward surface-enhanced Raman scattering (SERS).[6,17] In previous work, GNR supercrystals for SERS detection were obtained by standard drop-casting, resulting in nonuniform supercrystal arrays, which strongly hinders the reproducibility of the experiments. In this work, we took advantage of the uniform distribution of supercrystals on the substrate, as well as the smectic order of the GNR and the control on the supercrystals' morphology. Supercrystal arrays were prepared on a glass substrate from a GNR colloid with a concentration of 75 mM. The patterned substrates were then cleaned with a combination of oxygen plasma and exposure to UV/ozone to remove the organic layer formed on top of the supercrystal surface, which would undoubtedly interfere with SERS detection (see Experimental Section). Oxygen plasma etching time was optimized to successfully remove the organic layer while avoiding any damage or reshaping of the GNRs (which was observed for longer exposure time; see Figure S11). Crystal violet (CV) was selected as a model analyte for SERS detection, and the measurements were carried out for supercrystals with different geometries. SERS images were acquired by mapping the spatial dependence of SERS intensity integrated over the shift range of 1618−1632 cm^{-1} (Figure 5). From these measurements, we can clearly see that the analyte could be detected on the supercrystals only, confirming the signal enhancement by the plasmon excitation of the nanorod assembly. Importantly, only the chemical fingerprint of the analyte was measured and the SERS signal intensity was uniform throughout the supercrystals' surface. Considering the low integration time of 500 ms and the low laser intensity (0.15 mW), an enhancement factor was determined to be 3.1 × 10^5 at 633 nm. This should be taken as a lower estimate as CV molecules are likely to deposit also on the substrate outside the supercrystals. Interestingly, we did not notice any changes on the multiscale organization of the patterned substrates after Raman experiments and further cleaning (Figure S12), thus allowing its reusability.[6]

Similar SERS experiments were carried out on supercrystals obtained with spheres and with large nanorods. Interestingly, we observed that larger nanorods (150 × 30 nm) provide higher signals, whereas spheres yield the lowest signals (Figure S13). This may be related to both the larger dimensions and the sharper tips of these nanorods. However, accurate comparison between different systems would require that the number of GNR layers be the same. Preliminary results indicate a significant dependence of the signal intensity with respect to the number of layers, in agreement with previous reports.[6]

CONCLUSIONS

In summary, a simple and reliable technique was devised to obtain nanoparticle supercrystal arrays by confining a gold nanoparticle colloid between a patterned PDMS mold and a flat substrate. Self-assembly takes place in one step on arbitrary substrates such as TEM grids, silicon wafers, and glass slides. The method only requires commercially available and inexpensive tools. The size, shape, and height of the obtained supercrystals can be regulated by varying the

mold cavity pattern and nanoparticle concentration. Overall, this technique is highly versatile, and the morphology of the supercrystals can be tuned with unprecedented control on the macroscale. SEM and TEM revealed the hierarchical order of the nanoparticles up to the millimeter scale. Supercrystal shaping was precise for all template geometries, opening new avenues for future development of complex structures. Furthermore, the three-dimensional features obtained in this work cannot be produced by other bottom-up techniques.[44,52] The macroscale assembly of different gold nanoparticle shapes and sizes was also demonstrated. We envision that the method can be applied to various colloids with different compositions, such as semiconductor nanoparticles or proteins, for a broad range of applications. Herein, the patterned substrates were used as a sensing platform, with a SERS response that was homogeneous and intense for the various supercrystal sizes and shapes. The size of the obtained supercrystals allows the use of larger laser spot size and thus of portable Raman spectrometers. Moreover, the high chemical stability of gold nanorods allowed us to store the substrates for months, which is important for the eventual fabrication of POC devices. Overall, the reproducibility, the fast optical read-out, the high sensitivity, together with the simplicity of fabrication, render these hierarchical assemblies appealing for the design of performing sensing platforms.

EXPERIMENTAL SECTION

Materials. All chemicals required for GNR synthesis and functionalization were purchased from Sigma-Aldrich unless otherwise indicated. All chemicals were used as received. Milli-Q water (resistivity 18.2 MΩ·cm at 25 °C) was used in all experiments.

GNR Synthesis. Pentatwinned gold nanorods (150 ± 15 nm length; 30 ± 3 nm width) were synthesized according to ref 53. Single-crystalline gold nanorods (55 ± 6 nm length; 17 ± 2 nm width) were synthesized through a seed-mediated method involving the prereduction of $HAuCl_4$ with salicylic acid.[46] Nanorods with an absorption maximum at 780 nm were obtained within 4 h after seed addition. The GNRs were then washed by centrifugation (7000 rpm, 40 min, 29 °C), and the pellet was redispersed in 0.05 M CTAB to remove excess reactants. The GNR concentration was expressed as Au molar concentration, calculated from the absorbance at 400 nm.[46] For MUDOL grafting, 5 mL of freshly made GNR solution was purified by centrifugation (7000 rpm, 40 min, 29 °C) from excess CTAB and dispersed in an equal volume of Milli-Q water to reach a final surfactant concentration of 1 mM. In a typical experiment, 5 mL of 0.2 mM MUDOL solution was then mixed with the purified GNR dispersion, shaken vigorously, and incubated for 24 h. The obtained MUDOL−GNRs were stable for months, and the concentration was adjusted between 15 and 375 mM by centrifugation (7000 rpm, 40 min, 29 °C and redispersion in the appropriate amount of water).

Mould Fabrication and 3D GNR Assembly. The microtextured mold was manufactured in PDMS (Sylgard 184, Dow Corning), following standard soft lithography techniques.[19,54] The master was composed of pillars having different shapes and sizes on a 4 in. silicon wafer covered with SU-8 resin. PDMS (10:1 elastomer to curing agent) was cured at 70 °C for 2 h. A drop (2 μL) of the chemically modified GNR dispersion was casted between a flat substrate and the microtextured surface and allowed to dry overnight in ambient conditions. Assembly experiments were performed on ⟨100⟩ silicon wafers, glass slides, and TEM grids (carbon-coated) without significant changes in the obtained degree of order, even if better assembly was observed on more hydrophilic substrates.

SERS Spectroscopy Characterization of the Patterned Substrates. Substrates were cleaned with a combination of oxygen plasma (2 min, 0.4 mbar, 200 W) and UV/ozone (1 h). Oxygen plasma surface treatment was performed in a low-pressure plasma system (PICO, Diener Electronic). UV/ozone surface treatment was performed in a UV/ozone cleaner (ProCleaner). A solution of crystal violet at 10^{-6} M in ethanol was drop-casted on the substrate and dried under ambient conditions. SERS measurements were performed on a commercial confocal scanning Raman microscope (micro-Renishaw InVia reflex system equipped with Peltier charge-coupled device detectors) using a 100× objective (NA = 0.85) with an excitation wavelength of 633 nm, 1200 lines/mm diffraction grating, $P \approx 0.15$ mW, integration time = 500 ms. Laser spot size was in the range of 1 μm in diameter.

SEM and Dark-Field Characterization. Dark-field microscopy images were obtained using a Nikon Eclipse Ti-U inversion optical microscope. SEM images of GNRs were obtained using an ESEM Quanta250 FEG (FEI, The Netherlands).

Conflict of Interest: The authors declare no competing financial interest.

Acknowledgment. This work was supported by the European Research Council (ERC Advanced Grant No. 267867 Plasmaquo). C.H. acknowledges the Direction Générale de L'Armement (DGA) for a postdoctoral fellowship (Grant No. PDE 13C003).

Supporting Information Available: Details on ligand exchange, including TEM histograms and UV−vis spectra, optical microscopy images of the PDMS template, SEM images of supercrystals from pentatwinned GNR and spheres, TEM image of the pentatwinned nanorods, influence of initial GNR concentration, determination of inter-nanorod spacing by TEM and AFM, influence of oxygen plasma etching, SEM of supercrystals after SERS experiments and cleaning, and comparison of crystal violet SERS spectra on supercrystals of different gold nanoparticle shapes. This material is available free of charge *via* the Internet at http://pubs.acs.org.

REFERENCES AND NOTES

1. Chen, W.; Weng, S.; Zhang, F.; Allen, S.; Li, X.; Bao, L.; Lam, R. H. W.; Macoska, J. A.; Merajver, S. D.; Fu, J. Nanoroughened Surfaces for Efficient Capture of Circulating Tumor Cells without Using Capture Antibodies. *ACS Nano* **2012**, *7*, 566–575.
2. Wang, S.; Liu, K.; Liu, J.; Yu, Z. T. F.; Xu, X.; Zhao, L.; Lee, T.; Lee, E. K.; Reiss, J.; Lee, Y.-K.; *et al.* Highly Efficient Capture of Circulating Tumor Cells by Using Nanostructured Silicon Substrates with Integrated Chaotic Micromixers. *Angew. Chem., Int. Ed.* **2011**, *50*, 3084–3088.
3. Yu, Z. T. F.; Aw Yong, K. M.; Fu, J. Microfluidic Blood Cell Sorting: Now and Beyond. *Small* **2014**, *10*, 1687–1703.
4. Engel, Y.; Schiffman, J. D.; Goddard, J. M.; Rotello, V. M. Nanomanufacturing of Biomaterials. *Mater. Today* **2012**, *15*, 478–485.
5. Moyano, D. F.; Rotello, V. M. Nano Meets Biology: Structure and Function at the Nanoparticle Interface. *Langmuir* **2011**, *27*, 10376–10385.
6. Alvarez-Puebla, R. A.; Agarwal, A.; Manna, P.; Khanal, B. P.; Aldeanueva-Potel, P.; Carbó-Argibay, E.; Pazos-Pérez, N.; Vigderman, L.; Zubarev, E. R.; Kotov, N. A.; *et al.* Gold Nanorods 3D-Supercrystals as Surface Enhanced Raman Scattering Spectroscopy Substrates for the Rapid Detection of

Scrambled Prions. *Proc. Natl. Acad. Sci. U.S.A.* **2011**, *108*, 8157–8161.
7. Alam, R.; Lightcap, I. V.; Karwacki, C. J.; Kamat, P. V. Sense and Shoot: Simultaneous Detection and Degradation of Low-Level Contaminants Using Graphene-Based Smart Material Assembly. *ACS Nano* **2014**, *8*, 7272–7278.
8. Alvarez-Puebla, R. A.; Liz-Marzan, L. M. Traps and Cages for Universal SERS Detection. *Chem. Soc. Rev.* **2012**, *41*, 43–51.
9. Golightly, R. S.; Doering, W. E.; Natan, M. J. Surface-Enhanced Raman Spectroscopy and Homeland Security: A Perfect Match? *ACS Nano* **2009**, *3*, 2859–2869.
10. Nie, S.; Emory, S. R. Probing Single Molecules and Single Nanoparticles by Surface-Enhanced Raman Scattering. *Science* **1997**, *275*, 1102–1106.
11. Aćimović, S. S.; Ortega, M. A.; Sanz, V.; Berthelot, J.; Garcia-Cordero, J. L.; Renger, J.; Maerkl, S. J.; Kreuzer, M. P.; Quidant, R. LSPR Chip for Parallel, Rapid, and Sensitive Detection of Cancer Markers in Serum. *Nano Lett.* **2014**, *14*, 2636–2641.
12. Arnold, M.; Schwieder, M.; Blummel, J.; Cavalcanti-Adam, E. A.; Lopez-Garcia, M.; Kessler, H.; Geiger, B.; Spatz, J. P. Cell Interactions with Hierarchically Structured Nano-patterned Adhesive Surfaces. *Soft Matter* **2009**, *5*, 72–77.
13. Ofir, Y.; Moran, I. W.; Subramani, C.; Carter, K. R.; Rotello, V. M. Nanoimprint Lithography for Functional Three-Dimensional Patterns. *Adv. Mater.* **2010**, *22*, 3608–3614.
14. Mérian, T.; Goddard, J. M. Advances in Nonfouling Materials: Perspectives for the Food Industry. *J. Agric. Food Chem.* **2012**, *60*, 2943–2957.
15. Vasilev, K.; Cook, J.; Griesser, H. J. Antibacterial Surfaces for Biomedical Devices. *Exp. Rev. Med. Dev.* **2009**, *6*, 553–567.
16. Kwiat, M.; Elnathan, R.; Kwak, M.; de Vries, J. W.; Pevzner, A.; Engel, Y.; Burstein, L.; Khatchtourints, A.; Lichtenstein, A.; Flaxer, E.; *et al.* Non-covalent Monolayer-Piercing Anchoring of Lipophilic Nucleic Acids: Preparation, Characterization, and Sensing Applications. *J. Am. Chem. Soc.* **2011**, *134*, 280–292.
17. Gómez-Graña, S.; Pérez-Juste, J.; Alvarez-Puebla, R. A.; Guerrero-Martínez, A.; Liz-Marzán, L. M. Self-Assembly of Au@Ag Nanorods Mediated by Gemini Surfactants for Highly Efficient SERS-Active Supercrystals. *Adv. Opt. Mater.* **2013**, *1*, 477–481.
18. Gates, B. D.; Xu, Q.; Stewart, M.; Ryan, D.; Willson, C. G.; Whitesides, G. M. New Approaches to Nanofabrication: Molding, Printing, and Other Techniques. *Chem. Rev.* **2005**, *105*, 1171–1196.
19. Qin, D.; Xia, Y.; Whitesides, G. M. Soft Lithography for Micro- and Nanoscale Patterning. *Nat. Protoc.* **2010**, *5*, 491–502.
20. Henzie, J.; Barton, J. E.; Stender, C. L.; Odom, T. W. Large-Area Nanoscale Patterning: Chemistry Meets Fabrication. *Acc. Chem. Res.* **2006**, *39*, 249–257.
21. Vakarelski, I. U.; Marston, J. O.; Thoroddsen, S. T. Foam-Film-Stabilized Liquid Bridge Networks in Evaporative Lithography and Wet Granular Matter. *Langmuir* **2013**, *29*, 4966–4973.
22. Zhan, Z.; Lei, Y. Sub-100-nm Nanoparticle Arrays with Perfect Ordering and Tunable and Uniform Dimensions Fabricated by Combining Nanoimprinting with Ultrathin Alumina Membrane Technique. *ACS Nano* **2014**, *8*, 3862–3868.
23. Xia, Y.; Kim, E.; Whitesides, G. M. Micromolding of Polymers in Capillaries: Applications in Microfabrication. *Chem. Mater.* **1996**, *8*, 1558–1567.
24. Kim, E.; Xia, Y.; Whitesides, G. M. Polymer Microstructures Formed by Moulding in Capillaries. *Nature* **1995**, *376*, 3.
25. Kim, E.; Xia, Y.; Whitesides, G. M. Two- and Three-Dimensional Crystallization of Polymeric Microspheres by Micromolding in Capillaries. *Adv. Mater.* **1996**, *8*, 245–247.
26. Nie, Z. H.; Petukhova, A.; Kumacheva, E. Properties and Emerging Applications of Self-Assembled Structures Made from Inorganic Nanoparticles. *Nat. Nanotechnol.* **2010**, *5*, 15–25.
27. Doherty, M. D.; Murphy, A.; McPhillips, J.; Pollard, R. J.; Dawson, P. Wavelength Dependence of Raman Enhancement from Gold Nanorod Arrays: Quantitative Experiment and Modeling of a Hot Spot Dominated System. *J. Phys. Chem. C* **2010**, *114*, 19913–19919.
28. Hou, J.; Zhang, H.; Yang, Q.; Li, M.; Song, Y.; Jiang, L. Bio-Inspired Photonic-Crystal Microchip for Fluorescent Ultra-trace Detection. *Angew. Chem., Int. Ed.* **2014**, *53*, 5791–5795.
29. Peng, B.; Li, G.; Li, D.; Dodson, S.; Zhang, Q.; Zhang, J.; Lee, Y. H.; Demir, H. V.; Ling, X. Y.; Xiong, Q. Vertically Aligned Gold Nanorod Monolayer on Arbitrary Substrates: Self-Assembly and Femtomolar Detection of Food Contaminants. *ACS Nano* **2013**, *7*, 5993–6000.
30. Fraire, J. C.; Pérez, L. A.; Coronado, E. A. Rational Design of Plasmonic Nanostructures for Biomolecular Detection: Interplay between Theory and Experiments. *ACS Nano* **2012**, *6*, 3441–3452.
31. Wei, W.; Chen, K.; Ge, G. Strongly Coupled Nanorod Vertical Arrays for Plasmonic Sensing. *Adv. Mater.* **2013**, *25*, 3863–3868.
32. Fan, M.; Andrade, G. F. S.; Brolo, A. G. A Review on the Fabrication of Substrates for Surface Enhanced Raman Spectroscopy and Their Applications in Analytical Chemistry. *Anal. Chim. Acta* **2011**, *693*, 7–25.
33. Zhou, Y.; Zhou, X.; Park, D. J.; Torabi, K.; Brown, K. A.; Jones, M. R.; Zhang, C.; Schatz, G. C.; Mirkin, C. A. Shape-Selective Deposition and Assembly of Anisotropic Nanoparticles. *Nano Lett.* **2014**, *14*, 2157–2161.
34. Zhou, X.; Zhou, Y.; Ku, J. C.; Zhang, C.; Mirkin, C. A. Capillary Force-Driven, Large-Area Alignment of Multi-segmented Nanowires. *ACS Nano* **2014**, *8*, 1511–1516.
35. Kuemin, C.; Nowack, L.; Bozano, L.; Spencer, N. D.; Wolf, H. Oriented Assembly of Gold Nanorods on the Single-Particle Level. *Adv. Funct. Mater.* **2012**, *22*, 702–708.
36. Malaquin, L.; Kraus, T.; Schmid, H.; Delamarche, E.; Wolf, H. Controlled Particle Placement through Convective and Capillary Assembly. *Langmuir* **2007**, *23*, 11513–11521.
37. Yin, Y.; Lu, Y.; Gates, B.; Xia, Y. Template-Assisted Self-Assembly: A Practical Route to Complex Aggregates of Monodispersed Colloids with Well-Defined Sizes, Shapes, and Structures. *J. Am. Chem. Soc.* **2001**, *123*, 8718–8729.
38. Thai, T.; Zheng, Y.; Ng, S. H.; Mudie, S.; Altissimo, M.; Bach, U. Self-Assembly of Vertically Aligned Gold Nanorod Arrays on Patterned Substrates. *Angew. Chem., Int. Ed.* **2012**, *51*, 8732–8735.
39. Alba, M.; Pazos-Perez, N.; Vaz, B.; Formentin, P.; Tebbe, M.; Correa-Duarte, M. A.; Granero, P.; Ferré-Borrull, J.; Alvarez, R.; Pallares, J.; *et al.* Macroscale Plasmonic Substrates for Highly Sensitive Surface-Enhanced Raman Scattering. *Angew. Chem., Int. Ed.* **2013**, *52*, 6459–6463.
40. Ahmed, S.; Ryan, K. M. Self-Assembly of Vertically Aligned Nanorod Supercrystals Using Highly Oriented Pyrolytic Graphite. *Nano Lett.* **2007**, *7*, 2480–2485.
41. Hamon, C.; Postic, M.; Mazari, E.; Bizien, T.; Dupuis, C.; Even-Hernandez, P.; Jimenez, A.; Courbin, L.; Gosse, C.; Artzner, F.; *et al.* Three-Dimensional Self-Assembling of Gold Nanorods with Controlled Macroscopic Shape and Local Smectic B Order. *ACS Nano* **2012**, *6*, 4137–4146.
42. Yilmaz, C.; Cetin, A. E.; Goutzamanidis, G.; Huang, J.; Somu, S.; Altug, H.; Wei, D.; Busnaina, A. Three-Dimensional Crystalline and Homogeneous Metallic Nanostructures Using Directed-Assembly of Nanoparticles. *ACS Nano* **2014**, *8*, 4547–4558.
43. Vakarelski, I. U.; Chan, D. Y. C.; Nonoguchi, T.; Shinto, H.; Higashitani, K. Assembly of Gold Nanoparticles into Microwire Networks Induced by Drying Liquid Bridges. *Phys. Rev. Lett.* **2009**, *102*, 058303.
44. Xu, L.; Ma, W.; Wang, L.; Xu, C.; Kuang, H.; Kotov, N. A. Nanoparticle Assemblies: Dimensional Transformation of Nanomaterials and Scalability. *Chem. Soc. Rev.* **2013**, *42*, 3114–3126.
45. Ye, X.; Jin, L.; Caglayan, H.; Chen, J.; Xing, G.; Zheng, C.; Doan-Nguyen, V.; Kang, Y.; Engheta, N.; Kagan, C. R.; *et al.* An Improved Size-Tunable Synthesis of Monodisperse Gold Nanorods through the Use of Aromatic Additives. *ACS Nano* **2012**, *6*, 2804–2817.

46. Scarabelli, L.; Grzelczak, M.; Liz-Marzán, L. M. Tuning Gold Nanorod Synthesis through Prereduction with Salicylic Acid. *Chem. Mater.* **2013**, *25*, 4232–4238.
47. Guerrero-Martínez, A.; Pérez-Juste, J.; Carbó-Argibay, E.; Tardajos, G.; Liz-Marzán, L. M. Gemini-Surfactant-Directed Self-Assembly of Monodisperse Gold Nanorods into Standing Superlattices. *Angew. Chem., Int. Ed.* **2009**, *48*, 9484–9488.
48. Xie, Y.; Guo, S.; Ji, Y.; Guo, C.; Liu, X.; Chen, Z.; Wu, X.; Liu, Q. Self-Assembly of Gold Nanorods into Symmetric Superlattices Directed by OH-Terminated Hexa(ethylene glycol) Alkanethiol. *Langmuir* **2011**, *27*, 11394–11400.
49. Deegan, R. D.; Bakajin, O.; Dupont, T. F.; Huber, G.; Nagel, S. R.; Witten, T. A. Capillary Flow as the Cause of Ring Stains from Dried Liquid Drops. *Nature* **1997**, *389*, 827–829.
50. Pietra, F.; Rabouw, F. T.; Evers, W. H.; Byelov, D. V.; Petoukhov, A.; de Mello Donegá, C.; Vanmaekelbergh, D. Semiconductor Nanorod Self-Assembly at the Liquid/Air Interface Studied by *In Situ* GISAXS and *Ex Situ* TEM. *Nano Lett.* **2012**, *12*, 5515–5523.
51. Ming, T.; Kou, X.; Chen, H.; Wang, T.; Tam, H.-L.; Cheah, K.-W.; Chen, J.-Y.; Wang, J. Ordered Gold Nanostructure Assemblies Formed by Droplet Evaporation. *Angew. Chem., Int. Ed.* **2008**, *120*, 9831–9836.
52. Zhang, S.-Y.; Regulacio, M. D.; Han, M.-Y. Self-Assembly of Colloidal One-Dimensional Nanocrystals. *Chem. Soc. Rev.* **2014**, *43*, 2301–2323.
53. Pérez-Juste, J.; Liz-Marzán, L. M.; Carnie, S.; Chan, D. Y. C.; Mulvaney, P. Electric-Field-Directed Growth of Gold Nanorods in Aqueous Surfactant Solutions. *Adv. Funct. Mater.* **2004**, *14*, 571–579.
54. McDonald, J. C.; Duffy, D. C.; Anderson, J. R.; Chiu, D. T.; Wu, H.; Schueller, O. J. A.; Whitesides, G. M. Fabrication of Microfluidic Systems in Poly(dimethylsiloxane). *Electrophoresis* **2000**, *21*, 27–40.